

# An improved monolithic multigrid Fluid-Structure Interaction solver with a new moving mesh technique

D. Cerroni , S. Manservigi and F. Menghini

**Abstract**—Fluid-Structure Interaction simulations have gained popularity in the research community because of their applications in several industrial and biological fields. In such problems mesh movement is necessary in order to clearly evaluate the deformed solid state and the stresses. In many cases, especially when large displacement occurs, the movement of the mesh nodes can reduce accuracy and convergence properties of the solver. In this paper we present an improved fluid structure interaction solver with a new moving mesh algorithm based on a multilevel Arbitrary Lagrangian Eulerian method to be used in the computation of the arbitrary fluid displacement field. This algorithm is used together with a multigrid, monolithic, fluid structure interaction solver for large displacement problem in which the mesh overlapping is more likely to happen. Numerical simulations in two and three-dimension for both hexahedral and tetrahedral meshes are reported in order to better investigate the capabilities of this solver.

**Keywords**- Fluid Structure Interaction, Arbitrary Lagrangian Eulerian, Monolithic solver, Multigrid solver.

## I. INTRODUCTION

IN recent years, numerical solution of Fluid-Structure Interaction problems has become of great interest because these simulations can be used in many applications ranging from nuclear technology to medicine. It is very common in nature to find Fluid-Solid interactions and the study of these problems can help design of components undergoing vibrations or tools needed for biological activities [1, 2]. The simulation of more complex problems in Computational Fluid Dynamics (CFD) has been made possible because of the development of efficient computational techniques and strong improvement in computer performance. However the solution of a Fluid-Structure Interaction (FSI) problem when large displacements are taken into account still remains a difficult task [1, 2, 3, 4]. Several methods have been proposed to deal with moving meshes in FSI. The most used one describes the solid motion in a Lagrangian framework while, as it is usually, the fluid is treated with an Eulerian approach. This technique lead to an Arbitrary Lagrangian-Eulerian (ALE) formulation which allows the coupling of fluid and structural simulations [5]. Mesh movement is necessary to define the boundary of a solid moving in a fluid. In the solid region we use a Lagrangian approach and the solid motion is defined by the elocity field while, in the fluid domain, the displacement field

is arbitrary and must be continuous at the solid-fluid interface. It is important to deform the fluid meshes uniformly avoiding point overlapping. This is usually achieved by imposing the displacement field of the solid part as a Dirichlet boundary condition for a Laplace problem solved on the fluid domain. Such approach prevents the fluid nodes from overcame each other when the characteristic dimension of the element are large enough but a refinement of the mesh, needed for an improved solution, increases the possibility of mesh overlapping. Moreover, in order to obtain a good solution, a fine mesh resolving the boundary layers on fluid-solid interfaces is needed [6]. Unfortunately tiny elements easily overlap when large displacements take place in the solid region. In order to improve the solution quality without increasing the risk of mesh overlapping, we propose a multilevel algorithm based on a multilevel Laplace operator. In standard ALE method the displacement field is the solution of an homogeneous Laplace problem with boundary conditions imposed by the real solid displacement. The new approach presented in this paper is based on the evaluation of the fluid displacement on the coarsest mesh and interpolation of this solution on the finer grids. Standard midpoint-refinement is used to obtain the finer meshes.

## II. MATHEMATICAL MODEL

### A. The fluid and solid modeling

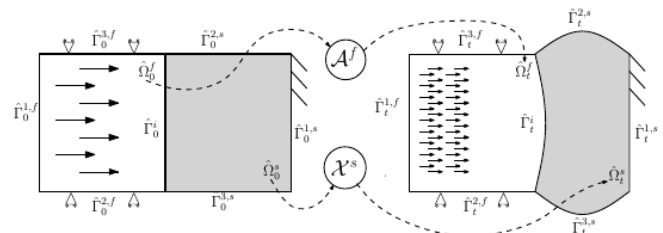


Fig. 1: Domain geometry. Fluid structure interaction reference and current deformed configurations.

In this section we introduce the notation that is used in order to describe current and reference configuration in fluid and solid domains. In an ordinary FSI problem we consider a mechanical system composed by a laminar Newtonian fluid region and a solid one which defines a moving domain  $\Omega_t$ . A schematic geometry of the problem is shown in Fig. 1. Let  $\Omega_t^f$

and  $\Omega_t^s$  be the fluid and the solid region at  $t \in (0, T]$ , respectively. At the time  $t = 0$  the fluid and solid region are defined by  $\Omega_0^f$  and  $\Omega_0^s$ . Let  $\Gamma_t^i = \Omega_t^f \cap \Omega_t^s$  and  $\Gamma_0^i = \Omega_0^f \cap \Omega_0^s$  be the interface where solid and fluid interact.  $\Gamma_t^k, k = 1, 2, 3$  and  $\Gamma_0^k, k = 1, 2, 3$  are defined to be the remaining external boundaries at  $t \in (0, T]$  and  $t = 0$ , respectively. The evolution of the solid and fluid domain  $\Omega_t^f$  and  $\Omega_t^s$  are defined by

$$\begin{aligned} X^s: \widehat{\Omega}_0^s \times \mathbb{R}^+ &\rightarrow \mathbb{R}^3, \\ A^f: \widehat{\Omega}_0^f \times \mathbb{R}^+ &\rightarrow \mathbb{R}^3, \end{aligned}$$

such that the range of  $X^s(\cdot, t)$  and  $A^f(\cdot, t)$  define  $\Omega_t^s$  and  $\Omega_t^f$ , respectively.  $X^s$  maps any material point  $x_0^s$  from the given fixed reference configuration  $\Omega_0^s$  to the current solid material configuration  $\Omega_t^s$ . The solid displacement is then defined as

$$\widehat{u}^s(\widehat{x}_0^s, t) = X(\widehat{x}_0^s, t) - \widehat{x}_0^s \quad (1)$$

The mapping  $A_f$  is such that  $A_f(x_0^f, t) = x_0^f + u^f(x_0^f, t)$ , where  $u^f(x_0^f, t)$  is defined as an arbitrary extension operator over the fluid domain  $\Omega_0^f$  and given by

$$\widehat{w}^f(\widehat{x}_0^f, t) = Ext(\widehat{u}^s|_{\Gamma_0^f}, t) \text{ in } \widehat{\Omega}_0^f \quad (2)$$

For details one can see [5, 7]. The behavior of the fluid is described by the Navier-Stokes equations of incompressible flows [8]

$$\left\{ \begin{aligned} \rho^f \frac{\partial v^f}{\partial t} + \rho^f (u^f - w^f) \cdot \nabla v^f - \nabla \cdot \sigma &= 0 \text{ in } (0, t) \times \Omega_t^f \\ \nabla \cdot v^f &= 0 \text{ in } (0, t) \times \Omega_t^f, \\ v^f|_{t=0} &= v_0 \text{ in } \widehat{\Omega}_0^f, \\ v^f|_{\Gamma_{t,D}^1 \cup \Gamma_{t,D}^2} &= g^f \text{ in } (0, t), \\ \sigma_f \cdot n^f|_{\Gamma_{t,D}^1 \cup \Gamma_{t,D}^2} &= h^f \text{ in } (0, t). \end{aligned} \right. \quad (3)$$

where  $\rho^f$  is the constant density,  $v^f$  is the fluid velocity and  $w^f$  denotes the fluid domain velocity.  $n$  is the unit normal vector that points outward from the boundary  $\partial\Omega_t^f$  and  $g^f, h^f, v_0$  are given data. The variables that determine the state of the flow in the incompressible case are the pressure  $p^f$  and the velocity  $v^f$ . The contribution of external forces like gravity is assumed to be negligible. The constitutive relation for the stress tensor in the Newtonian incompressible case reads

$$\sigma^f = -p^f I + \tau^f = -p^f I + 2\mu^f \epsilon(v^f) \quad (4)$$

where  $\mu^f$  is the dynamic viscosity of the fluid,  $p^f$  the Lagrange multiplier associated to the incompressibility constraint and  $\epsilon(v^f)$  the strain rate tensor defined as

$$\epsilon(v^f) = \frac{1}{2}(\nabla v^f + (\nabla v^f)^t). \quad (5)$$

The material time derivative is related to the adopted reference systems.

The governing equations for structural mechanics are the following momentum equations

$$\rho^s \left( \frac{\partial v^s}{\partial t} + v^s \cdot (\nabla v^s) \right) - \nabla \cdot \sigma^s(u^s) = 0 \text{ in } \Omega_t^s \quad (6)$$

where  $\rho^s$  is the density of the material,  $v^s$  is the velocity field and  $\sigma^s$  is the Cauchy stress tensor, which is a function of the

displacement  $u^s$  of the structure. Since the constitutive law for the solid stress tensor is expressed in terms of displacements one must solve both the balance equations (6) and the kinematic relation

$$v^s = \frac{\partial u^s}{\partial t} \quad (7)$$

For the reference configuration we can introduce the right Cauchy-Green deformation tensor  $C$  as

$$C = F^t \cdot F, \quad (8)$$

where  $F$  is the deformation gradient tensor defined by  $F = I + \nabla u^s$ . In a similar way in the current configuration we can introduce the left Cauchy-Green deformation tensor,  $b$ , as

$$b = F \cdot F^t. \quad (9)$$

According with this notation we can now express the Cauchy stress tensor,  $\sigma^s$ , as [9]

$$\frac{2}{J} [b_{ij} (I b_{ij} - b_{im} b_{mj}) \frac{J \delta_{ij}}{2}] \begin{pmatrix} \frac{\partial W}{\partial I} \\ \frac{\partial W}{\partial II} \\ \frac{\partial W}{\partial J} \end{pmatrix} \quad (10)$$

where  $I = \text{tr}C$ ,  $II = \text{tr}(C^2) - (\text{tr}C)^2$  are the first and second invariant of the right Cauchy-Green strain tensor  $C$  and  $J$  its determinant. The quantity  $W = W(I, II, J)$  is the strain energy of the system which depends on the constitutive law of the considered material. For example for a Neo-Hookean material, with respect of the current configuration, the energy function is defined by

$$\begin{aligned} W(I, J) &= \left( \frac{1}{2} \mu_s J^{-2/3} \text{tr}(C) - 3 \right) \\ &+ \frac{1}{2} \left( \lambda + \frac{2}{3} \mu_s \right) \left( \frac{1}{2} (J^2 - 1) - \ln(J) \right) \end{aligned} \quad (11)$$

The interested reader can consult [9].

### B. The coupled fluid-structure model

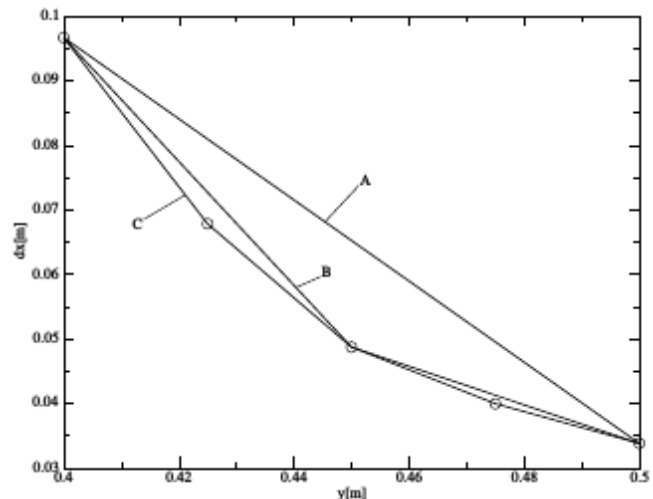


Fig. 2: Quadratic hexahedral element displacement for a two level solution: A is the displacement obtained with the proposed method, B is the standard one-level solution and C the displacement obtained with a standard ALE.

The fluid and solid problem defined by (3) and (6) are well posed when we prescribe appropriate boundary conditions. In the case where the fluid and the solid regions have a common

boundary  $\Gamma_t^i$  it is necessary to specify boundary conditions at this interface. The coupling between the fluid and the solid model is set by these boundary conditions which also define the nature of their interactions. Usually one can impose the velocity and the stress at the interface  $\Gamma_t^i$  by setting

$$\begin{aligned} v^f|_{\Gamma_t^i} &= v^s|_{\Gamma_t^i} \\ \sigma^f \cdot n^f|_{\Gamma_t^i} + \sigma^s \cdot n^s|_{\Gamma_t^i} &= 0 \end{aligned}$$

With these assumptions the fluid structure coupled state  $(v, p, u)$  for a compressible solid and fluid satisfies the following complete set of equations

$$\left\{ \begin{aligned} \rho^f \frac{\partial v^f}{\partial t} + \rho^f (u^f - w^f) \cdot \nabla v^f + \nabla p - \nabla \cdot \tau^f &= 0 \quad \text{in } \Omega_t^f \\ \nabla \cdot v^f &= 0 \quad \text{in } \Omega_t^f, \\ \rho^s \frac{\partial v^s}{\partial t} - \nabla \cdot \tau^s &= 0 \quad \text{in } \hat{\Omega}_0^s, \\ v &= \frac{\partial u}{\partial t} \quad \text{in } \hat{\Omega}_t^s \\ \frac{\partial u^f}{\partial t} - k \Delta u &= 0 \quad \text{in } \Omega_t^f \\ u^f &= u^s \quad \text{in } \Gamma_t^i \\ w &= \frac{\partial u}{\partial t} \quad \text{in } \Omega_t^f \end{aligned} \right. \quad (14)$$

with the initial conditions

$$\begin{aligned} u(x_0, 0) &= u_0 \quad \text{in } \Omega_0, \\ v(x_0, 0) &= v_0 \quad \text{in } \Omega_0. \end{aligned}$$

In order to approximate the solution of the system (14) with finite element method we need the variational formulation of the problem. This formulation can be obtained by the usual technique by multiplying the equations (14) and using appropriate test functions [9]. By taking into account boundary and interface conditions we can integrate by parts and obtain the monolithic coupled formulation of this FSI problem. The extension operator more commonly used to evaluate the fluid region displacement is the harmonic or Laplace operator. In this case the fluid displacement  $u^f$  is defined by the solution of the following elliptic problem

$$\begin{aligned} \frac{\partial u^f}{\partial t} - k \Delta u &= 0 \quad \text{in } \Omega_t^f \\ u^f &= u^s \quad \text{in } \Gamma_t^i \end{aligned}$$

where  $k$  is the diffusion coefficient [1, 5, 9]. Other choices for the extension operator can be used. For details one can see [10]. Now we can define the velocity  $w^f$  of the points of the fluid domain in the current configuration. The velocity  $w^f$  is defined by

$$w^f = \frac{\partial u^f}{\partial t} \quad \text{in } \Omega_t^f.$$

This quantity represents the velocity in terms of the reference coordinate  $x_0$ . We remark that the displacement of the fluid domain is completely arbitrary and it is meant to avoid mesh overlapping. In order to improve the computation of the fluid displacement field, we propose a new method to combine the solution of the Laplace problem at different mesh

resolutions. The meshes are based on the Taylor Hoods elements [11]. The main idea is to use a multilevel scheme based on the linear points of the coarse level elements in order to interpolate linearly the solution on all the remaining points of the domain. In the next section we introduce several tests to prove that this algorithm prevents large fluid domain distortion and point overlapping. For a better explanation of the algorithm let us consider the displacement of a mono-dimensional quadratic element in a two-level solution. The coarse level grid is composed by three nodes and the two boundaries points are the linear nodes. The finer level grid consists of five nodes obtained by adding a node between each pair of the coarse level grid. In Figure 2 the curve C represents an example of the displacement solution evaluated in all the quadratic points of the finer level. As one can see the displacement of the first point is much greater than the one of the second point because of the nature the Laplace equation solution. This is the principal cause of the mesh overlapping. The curve B is the same previous solution projected in the coarser grid, we can notice that in such case the displacement of the nodes belonging to the finest level increase reducing the possibility of mesh overlapping. However it is clear that the linear interpolation of the solution between the linear nodes of the coarser grid increases the displacement of the most of the points of the element and, as a consequence, highly reduces the possibility of the mesh overlap.

### III. NUMERICAL RESULTS

In this section we test the multilevel mesh moving technique and compare the solution obtained with a standard ALE with the one obtained with this new method for both triangular and hexahedral meshes.

#### A. Test 1

Solid		Liquid	
Property	value	Property	value
E	$1 \times 10^4 Pa$	$\mu$	$1 \times 10^{-3} Pa \cdot s$
$\rho_s$	$1000 Kg/m^3$	$\rho_l$	$1000 Kg/m^3$
$\nu$	0.4		

Table 1: Test 1. Physical data for the Neo-Hookian material and the fluid.

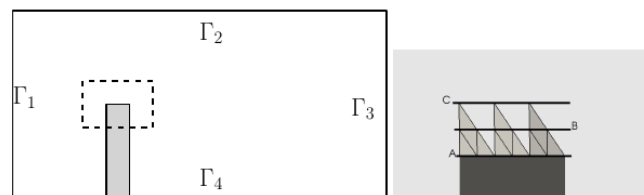


Fig. 3: Test 1. Domain overview (on the left) and locations of reference points (on the right).

In Test 1 we consider the bending of a rod due the transverse fluid velocity field as shown on the left of Figure 3 where one can see the problem domain  $\Omega_f \cup \Omega_s$  and the

boundary regions  $\Gamma_1$ ,  $\Gamma_2$ ,  $\Gamma_3$  and  $\Gamma_4$ . For the solid and liquid regions, we consider a compressible Neo-Hookean material and an incompressible fluid with properties shown in the Table 1, respectively. The fluid flow enters from  $\Gamma_1$  with constant velocity  $u_f = 1\text{m/s}$  and leaves the domain through  $\Gamma_3$  where free outflow condition is imposed. On the rest of the boundary  $\Gamma_2$  and  $\Gamma_4$  no-slip boundary conditions are set. The location of the points of interest (belonging to the lines A, B, C) is shown on the right of Figure 3. The line A corresponds to the solid-fluid interface. The line B contains the fluid

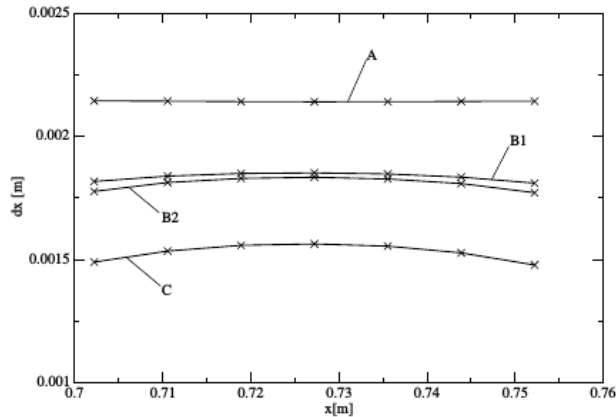


Fig. 4: Test 1. Reference point displacement belonging to the line A, B, C. B2 is the displacement obtained with a standard ALE and B1 is the one obtained with the proposed algorithm.

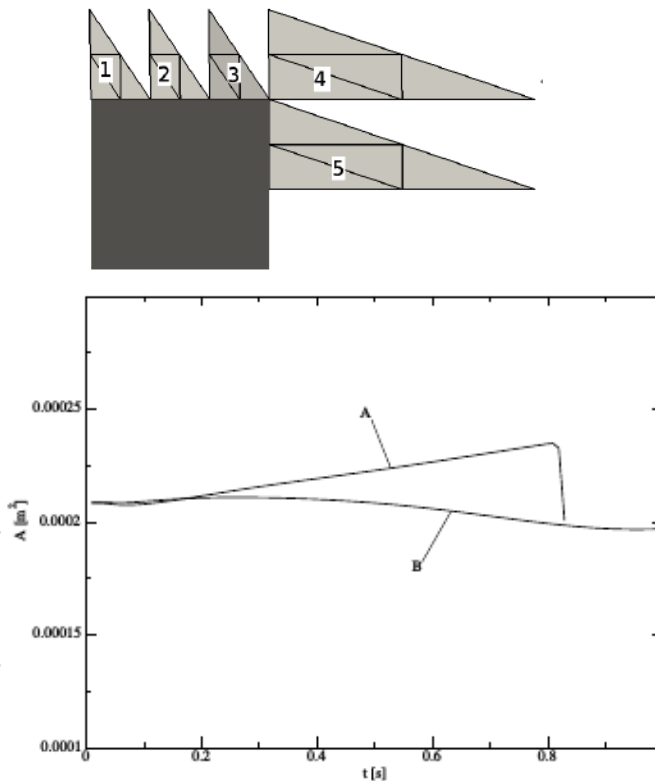


Fig. 5: Test 1. Reference elements (1, 2, 3, 4, 5) on the top and area of the element 1 over time on the bottom with the standard ALE (A) and with the proposed ALE algorithm (B).

triangular side midpoints (quadratic nodes) while the points on

the line C are the fluid triangle vertices (linear and quadratic nodes). The solution of this problem is obtained by solving the fluid displacement with a one-level algorithm based on a triangular mesh with two different moving approaches. In standard ALE method all the points, vertices and midpoints, are moved as solution of the Laplace operator, while in the new proposed approach the midpoint displacements are obtained by linear interpolation over the vertex points. A comparison between the displacements belonging to the lines A, B, C, in the longitudinal direction, is shown in Fig. 4. The displacement on the line A and C is the same while substantial differences can be seen over the middle point curve B. B1 and B2 are the displacements obtained, for the first time step, with the proposed and standard ALE, respectively.

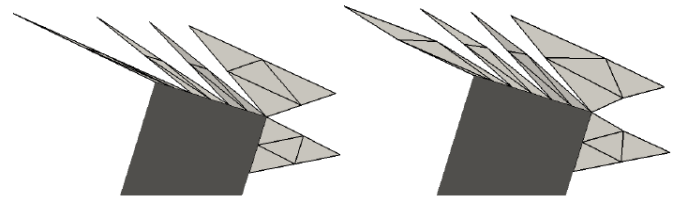


Fig. 6: Test 1. Deformed mesh with the proposed method (on the left) and with the standard ALE (on the right) with one-level mesh.

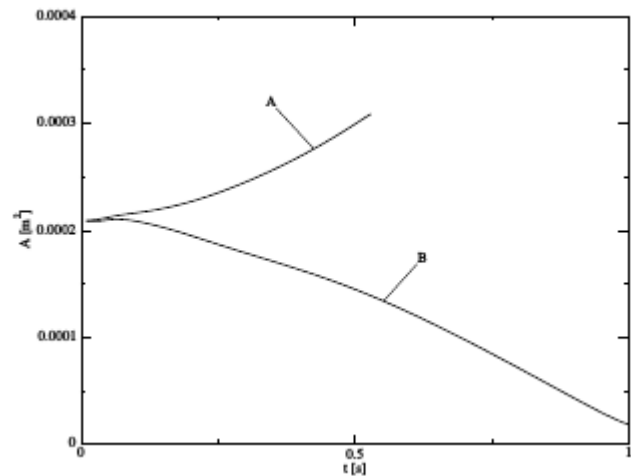


Fig. 7: Test 1. Area of the element 3 as a function of time for the standard ALE (A) and the new method (B) with two-level mesh.

From this one can see how the same point moves differently in agreement with the approach used. As an indicator of the mesh quality we consider the variation of the computational element area. The area and the corresponding triangle labels are shown on the left of Fig. 5. On the right of Fig. 5 the evolution of the area of the triangular element 1 is reported for the standard (A) and new (B) ALE algorithm. In particular we can see that with the standard ALE, due to the boundary effect of the Laplace solution, the area of the element becomes different from the initial one and it overlaps over another element destroying the mesh integrity. With the new algorithm, because of the smoothness of the solution, this effect is contained and the area of the element remains almost constant during the solid motion.

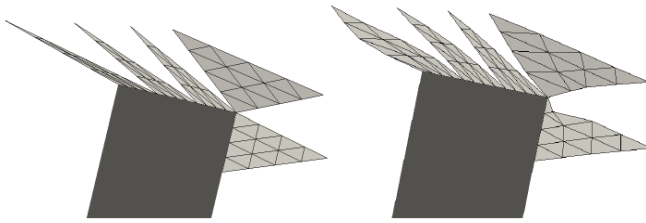


Fig. 8: Test 1. Deformed mesh with the proposed method (on the left) and with the standard ALE (on the right) with a two-level mesh.

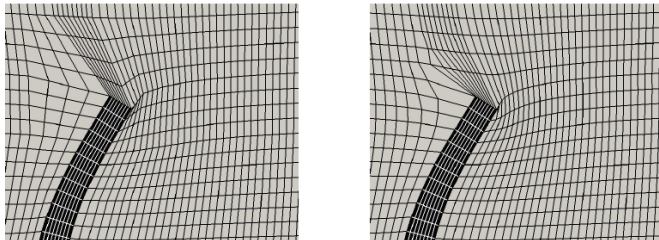


Figure 9: Test 1. Deformed mesh with the proposed method (on the top) and with the standard ALE (on the bottom) with a two-level hexahedral mesh.

On Fig. 6 the overview of the displaced mesh is shown for both cases for a one-level mesh algorithm. With the new ALE approach we obtain a more sharp deformation and the mesh is kept from overlapping till the steady state is reached. We perform again the same computation with a two-level mesh. The fine one is obtained by a mid-point refinement of the coarse mesh elements. From Fig. 7 we can see the evolution of the area of the element 3 and notice that the border effect of the Laplace solution is important and the area increases faster than the one obtained with the one level solution (Curve A). This is the opposite of what happens using the new interpolated ALE method (Curve B). We recall that, in one-level mesh, the new ALE algorithm interpolates the linear points to obtain the quadratic ones while, in a two-level mesh, all the points are computed as linear interpolation of the coarse vertices. On Figure 8 the overview of the displaced mesh for a two-level algorithm is shown for both ALE methods. We remark that the displaced mesh obtained with more levels and the proposed algorithm remains approximately uniform while the deformation of the one obtained with the standard algorithm tends to deform strongly. The Test 1 performed with the standard ALE cannot reach the steady state because of point overlapping. On the contrary the steady state can be easily reached by using the new technique. Analogous results could be obtained using an hexahedral mesh instead of a tetrahedral one.

An overview of the displaced mesh constructed with hexahedral mesh, for a two-level algorithm is shown in Fig. 9. In particular on the top we can notice the displaced mesh obtained with the interpolated ALE and on the bottom the one obtained with a standard ALE.

## B. Test 2

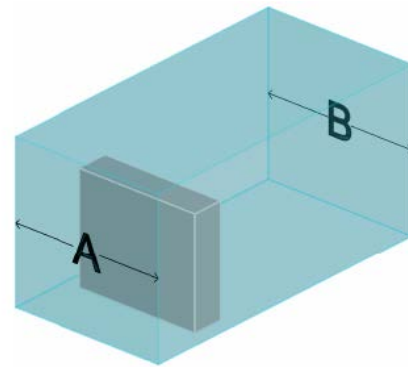


Figure 10: Test 2. Domain overview.

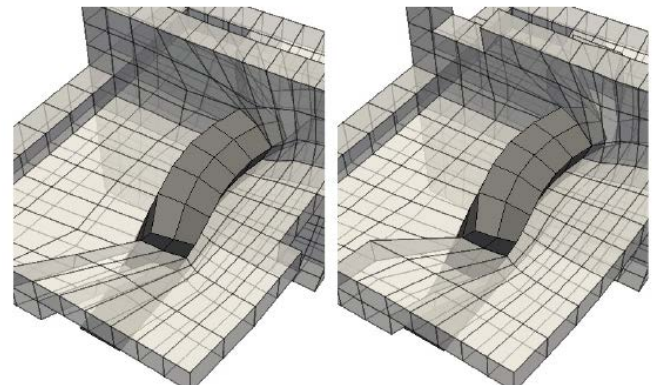


Figure 11: Test 2. Displaced mesh, obtained with a mono-level solver. Mesh moved with the proposed method (on the left) and with the standard ALE (on the right).

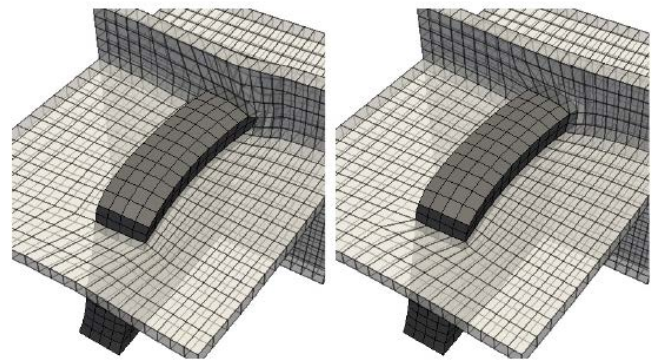


Figure 12: Test 2. Displaced mesh, obtained with a two level solver. Mesh moved with the proposed method (on the left) and with the standard ALE (on the right).

The second test is an extension of the previous one in a three-dimensional domain. In particular we consider the bending of a thin plate due to the transverse fluid motion. This test allows us to explore the behavior of the proposed method in three-dimensional geometry. The setup of the test is shown in Fig. 10 where the surface labeling is introduced. A is the

inlet surface where we impose the normal component of the velocity with constant value  $u_f = 1\text{m/s}$  and B is the outflow surface. In the remaining part of the boundary the velocity is set to zero. For the solid part we consider a compressible Neo-Hookean material with properties shown in the following table

Solid		Liquid	
Property	value	Property	value
E	$1 \times 10^4 Pa$	$\mu$	$1 \times 10^{-3} Pa \cdot s$
$\rho_s$	$1000 Kg/m^3$	$\rho_l$	$1000 Kg/m^3$
$\nu$	0.4		

Table 2: Test 2. Physical data for the Neo-Hookian material and the fluid.

The displaced mesh, obtained with a one-level algorithm, is shown in Fig.11. The mesh for the one-level algorithm consists of 8 vertices and 19 midpoints to form a typical Hex27 quadratic finite element. The 8 element vertices computed with the new ALE algorithm is moved in agreement with a three-dimensional Laplace problem while the 19 element midpoints are displacement is obtained with a linear interpolation. In particular, on the left, the mesh is displaced with the proposed approach and on the right with a standard ALE. An improved solution for the same problem is obtained by using a two-level mesh algorithm. In the new two-level mesh algorithm the displacement is computed only in the 8 vertices of the coarse mesh by solving the Laplace problem while all the others solutions are interpolated linearly. A comparison between the displaced mesh obtained with the two different methods can be seen in Fig. 12. From Figs. 11 and 12 one can note that the finer the mesh grid is in the the standard ALE, the greater are the boundary effect of the solution in the closest element on the Fluid structure interface. This is usually the element where overlapping occurs.

C. Test 3

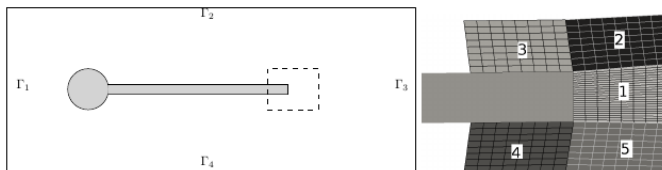


Figure 13: Test 3. FSI benchmark schematic (on the left) and reference elements near the tip of the tail of the solid part (1, 2, 3, 4, 5) (on the right).

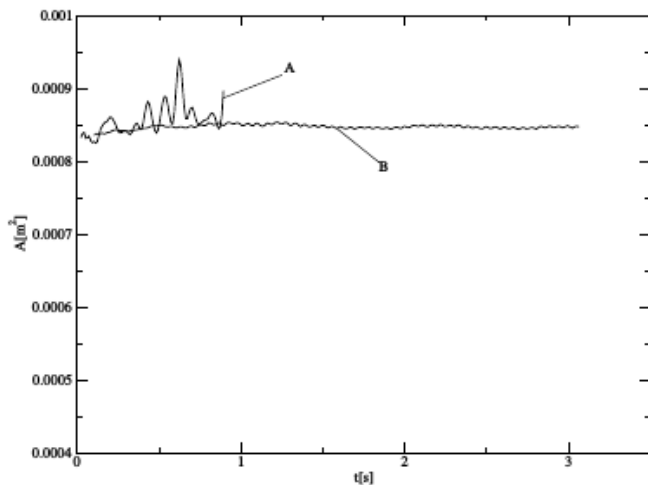


Figure 14: Test 1. Area of the element 1 over time with the standard ALE (A) and with the new ALE method (B).

In this example we test the behavior of the new algorithm for a three-level mesh movement. On the left part of the Fig. 13 we show the geometry of the problem taken from the Turek benchmark for large FSI deformation problems [12]. This is a two-dimensional flow in a channel past a fixed cylinder with a thin flexible bar attached to the downstream side of the cylinder.

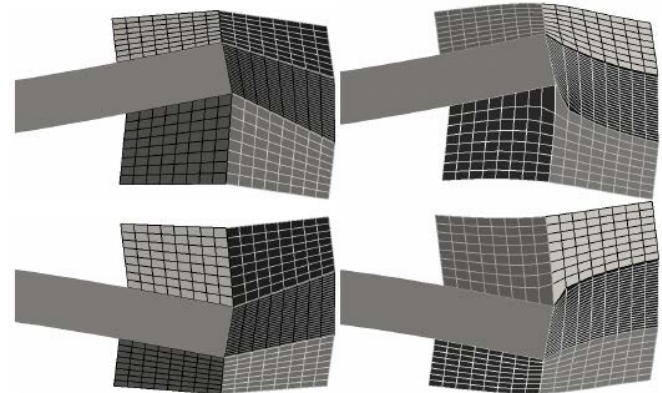


Figure 15: Test 3. Deformed mesh at different time steps (top , bottom) with the proposed (on the left) and the standard ALE method (on the right).

Property	value	Property	value
E	$1 \times 10^6 Pa$	$\mu$	$1 \times 10^{-3} Pa \cdot s$
$\rho_s$	$1000 kg/m^3$	$\rho_l$	$1000 kg/m^3$
$\nu$	0.4	$\langle v \rangle_0$	$20 m/s$

Table 3: Test 3. Physical data for the Neo-Hookian material and the fluid.

The test consists of laminar incompressible channel flow around an elastic object which results in self-induced asymptotic oscillations of the structure [13]. A and B are the inlet and outlet surfaces where we set the inlet velocity ( $u_f = 20m/s$ ) and outflow boundary condition, respectively. In the remaining part of the boundary the velocity is set to zero. For the solid part we consider an incompressible Neo-Hookian material with properties reported in Table 3. According to the previous notation on Fig. 14 we show the variation of the area of element 1 during time obtained with a standard ALE method (A) and with the proposed one (B). We can notice that with a standard ALE the oscillation of the solid leads to large deformation of the area of the nearest element of the liquid domain and the asymptotic periodical state could not be reached. Such deformations are hugely reduced using the proposed technique and the asymptotic periodical state is reached. In the top and the bottom part of Fig. 15 the displaced mesh is show at two different time steps in which the maximum displacement occurs, in particular in the left part we can observe the mesh displaced with the modified ALE and in the right part the one obtained with the standard technique.

## D. Test 4

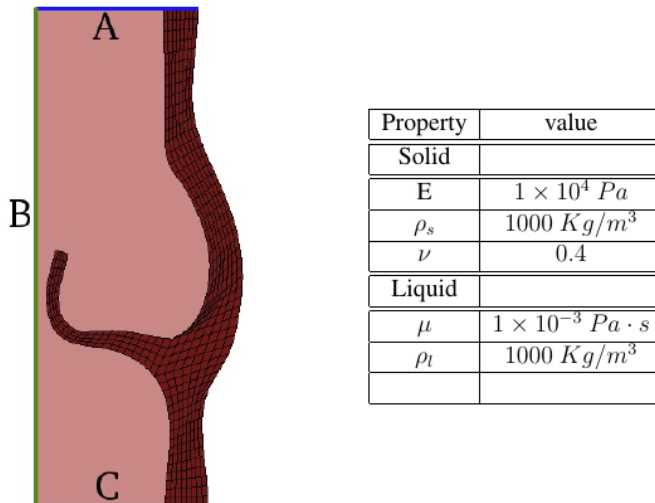


Figure 16: Test 4. Hart mitral valve schematic geometry (left) and physical data (right).

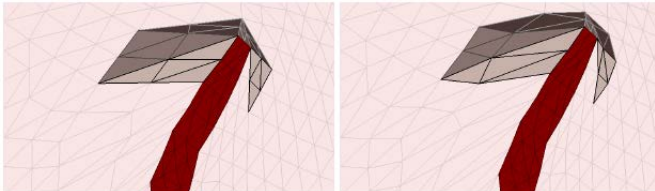


Figure 17: Test 4. Deformed triangular mesh obtained with the proposed method (on the left) and with the standard ALE (on the right). The colored part mark the finite elements of the domain.

In this last example we test the behavior of the proposed model in a complex geometry which aims to reproduce the movement of a section of the heart mitral valve. The geometry of the problem is shown in Fig. 16, where symmetry conditions are imposed on the surface B while homogeneous Neumann conditions are imposed on A. The blood flow is modeled as an incompressible fluid [14]. Over the inlet, denoted by C, the solid velocity is set to zero while the liquid velocity is time-dependent. This transient behavior simulates the blood flow coming from the atrium to the ventricle causing of the valve movement. The solid is modeled as an incompressible Neo-Hookian material with properties defined in Table 16. At the initial time the valve is closed and it is forced to open due to the increasing flow rate. In Fig. 17 the deformed triangular one-level mesh is shown near the fully open position. After this point, due to mesh deformation, only the new modified ALE method can reach the asymptotic periodical motion while the standard one failed. We perform the same computation for an hexahedral mesh. In the one level mesh no differences in the displacement field can be seen by using different algorithms. In Fig. 18 the deformed mesh, based on hexahedral elements, is shown for a two-level mesh with two different methods. In particular on the left and right part of the figure the mesh configuration obtained with the new algorithm is shown together with the one obtained with a standard ALE algorithm. In the same figure the element of different levels can be distinguished by colors. One can notice

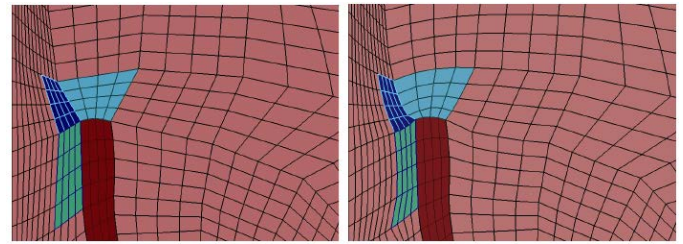


Figure 18: Test 4. Deformed quadrangular obtained with the proposed method (on the left) and with the standard ALE (on the right). The colored part mark the coarse element in the first level.

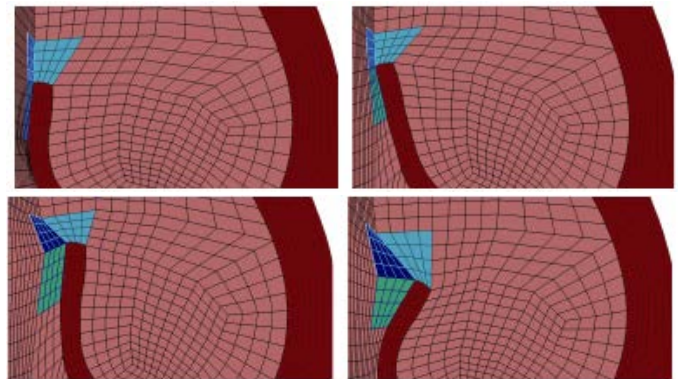


Figure 19: Test 4. Evolution of the mesh obtained with the proposed displacement algorithm at  $t = 0.3, 0.7, 1.1$  and  $1.6s$ .

that, by using the standard ALE method, the fluid interface is subject to large deformations that force the nodes to overlap. On the contrary interpolating the coarse displacement the shape of the element is preserved and the mesh nodes are prevent from collapsing. On Fig. 19 an overview of the mesh evolution, obtained with the proposed method, is shown at different time  $t = 0.3, 0.7, 1.1$  and  $1.6s$ . We remark that the same solution cannot be obtained with a standard ALE method because of point overlapping which occurs suddenly after the configuration shown in Fig. 18.

## IV. CONCLUSION

The mesh movement is necessary in fluid structure computation. In this work we have presented a multilevel algorithm to create an artificial displacement field in the fluid region and move consequently the mesh grid. In the first test we have shown the performance of the proposed algorithm in a simple two dimensional case. In the second test we have extended the previous analysis to the three dimensional problems and shown the differences between single and two-level ALE algorithm. Finally we have tested the high multi-level approach both in simple and complex geometries. In all the cases the proposed model shows a great stability and, differently from the standard ALE algorithm based on a single level, reduces substantially the point overlapping for arbitrary mesh movements. We show that the improvement is obtained considering both tetrahedral and hexagonal meshes.

## REFERENCES

- [1] E. Aulisa, A. Cervone, S. Manservigi and P. Seshaiyer, *A multilevel domain decomposition approach for studying coupled flow applications*, Commun. Comput. Phys., Vol.6, pp.319-341 2009.
- [2] E. Aulisa, S. Manservigi and P. Seshaiyer, *A multilevel domain decomposition approach to solving coupled applications in computational fluid dynamics*, International Journal for Numerical Methods in Fluids, Vol. 56(8), pp. 1139-1145, 2008.
- [3] L. Formaggia, A. Quarteroni and A. Veneziani, *Cardiovascular Mathematics*, Springer, 2009.
- [4] E. Aulisa, S. Manservigi and P. Seshaiyer, *A non-conforming computational methodology for modeling coupled problems*, Nonlinear Analysis, Volume 63, pp.1445-1454, 2005.
- [5] J. Donea, S. Giuliani and J. Halleux, *An Arbitrary Lagrangian Eulerian Finite Element Method for transient Fluid-Structure Interactions*. Comput. Meth. Appl. Mech. Eng. Vol.33,1982, pp. 689-723.
- [6] C. Arico, T. Tucciarielli, *Comparison of different 2nd order formulations for the solution of the 2D groundwater flow problem over irregular triangular meshes*, wseas transactions on fluid mechanics, Issue 2, Volume 4, April 2009.
- [7] P. Tallec and J. Mouro, *Fluid structure interaction with large structural displacements*, Computer Methods in Applied Mechanics and Engineering, 190, pp.24-25, pp. 3039-67, 2001.
- [8] Edisson Svio De Ges Maciel *A Review of Some Numerical Methods to the Euler Equations in Two-Dimensions*, wseas transactions on fluid mechanics, Issue 3, Volume 7, July 2012.
- [9] O.C. Zienkiewicz, R.L. Taylor and P. Nithiarasu, *The Finite Element Method for Fluid Dynamics*, Butterworth-Heinemann, Oxford, 2014.
- [10] P.A. Sackinger, P.R. Schunk and R.R. Rao, *A Newton-Raphson pseudo-solid domain mapping technique for free and moving boundary problems: a finite element implementation*, Journal of Computational Physics 125(1):83-103, 1996.
- [11] O. Zienkiewicz, R. Taylor and J.Z. Zhu *The Finite Element Method: Its Basis and Fundamentals*, ISBN9780080472775, Butterworth-Heinemann, 2005
- [12] S. Turek and J. Hron *Proposal for Numerical Benchmarking of Fluid-Structure Interaction between an Elastic Object and Laminar Incompressible Flow* Springer Berlin Heidelberg, P 371-385, 2006
- [13] S. Turek, J. Hron, *Proposal for Numerical Benchmarking of Fluid-Structure Interaction between an Elastic Object and Laminar Incompressible Flow*, Lecture Notes in Computational Science and Engineering, Volume 53, pp 371-385, 2006.
- [14] A. Mirza, A. R. Ansari, A.M. Siddiqui, T. Haroon *On the steady two-dimensional flow of blood with heat transfer in the presence of a stenosis*, wseas transactions on fluid mechanics, Issue 4, Volume 8, October 2013.